

ARTICLE OPEN



Future changes in atmospheric synoptic variability slow down ocean circulation and decrease primary productivity in the tropical Pacific Ocean

Olaf Duteil¹ and Wonsun Park^{2,3}

This study investigates the impact of future changes in atmospheric synoptic variability (ASV) on ocean properties and biogeochemical cycles in the tropical Pacific Ocean using coupled and forced atmosphere–ocean model experiments. Future climate projections show an annual mean decrease in ASV in subtropical gyres and an increase in the tropical band. Maintaining ASV to current values lead to a deepening of the mixed layer in subtropical regions and a shallowing at the equator associated with a sea surface temperature decrease. The changes in ASV impact the large-scale ocean circulation and the strength of the subtropical and tropical cells, which constrain the equatorial water upwelling and the tropical net primary productivity. Ultimately, this study highlights the significance of ASV in understanding the impacts of climate change on ocean dynamics and biogeochemical processes, as half of the primary productivity decline due to climate change is caused by changes of ASV in the tropical Pacific Ocean.

npj Climate and Atmospheric Science (2023)6:136; <https://doi.org/10.1038/s41612-023-00459-3>

INTRODUCTION

Climate change due to the increase of carbon dioxide in the atmosphere modifies the heat budget in the earth system, leading to changes in ocean properties, such as ocean surface temperature and stratification¹, as well as atmosphere properties, such as the surface wind field, a major forcing of ocean circulation. Changes in both atmosphere and ocean circulation ultimately reshape the distribution of key biogeochemical quantities such as ocean productivity^{2–5}.

Atmosphere circulation is characterized by different timescales of variability, ranging from sub-daily to multidecadal. Based on the 40 year's data from the fifth generation of ECMWF Re-reanalysis (ERA5), it has been shown that the “storm band” (period from 18 h to 1 month) or synoptic variability band^{6,7} captures most of the wind variance over the global ocean in mid-latitudes⁸. The atmospheric synoptic variability (ASV) is associated with storm tracks in mid- and high-latitudes and with extra-tropical cyclones^{7,9}. In tropical regions, the importance of the ASV is less prominent and displays a variance of the same order of magnitude compared to the annual cycle, or the El Niño/Southern Oscillation in the Pacific Ocean⁸. The trade winds are generally steadier than mid-latitude flows but still exhibit significant synoptic variability¹⁰. Close to the equator, important sources of the ASV are the Inter-Tropical Convergence Zone (ITCZ)¹¹, and the South Pacific Convergence Zone (SPCZ)¹². The location of the ITCZ and SPCZ controls the distribution of tropical cyclones^{12,13}, included in the ASV.

The ASV impacts ocean circulation and biogeochemical cycles as strong winds transfer mechanical energy to the upper ocean, modulate the surface heat fluxes¹⁴ and increase vertical mixing. Model experiments suggest that the accumulated effect of tropical cyclones in the current climate enhances productivity by up to 15% in the eastern tropical Pacific Ocean¹⁵. Storms enhance the net community production in mid-latitudes in summer due to nutrient injection from the deep ocean into the surface water¹⁶

and drive the outgassing of CO₂ in high latitudes, impacting the global carbon cycle¹⁷.

Filtering out the intra-monthly atmosphere variability (more specifically zonal and meridional wind velocity) in model experiments forced by the Japanese Reanalysis (JRA) 55 weakens the wind-driven ocean circulation by 10–15% in subtropical regions and the meridional overturning circulation by up to 50%¹⁸. Using a similar methodology another study¹⁹ filtered out the higher frequencies of wind variability in model experiments forced by the Coordinated Ocean-Ice Reference Experiments (CORE) v2 reanalysis. Wind stress decreased by up to 20% in the tropics and 50% in the mid-latitudes when a 1-month filter was applied, weakening ocean productivity by 20%.

The role of the ASV in modulating ocean properties is however still poorly understood, especially in a changing climate. While the average wind increases by 15% in tropical regions and decreases in the subtropics during the next century in CMIP5²⁰ and CMIP6²¹ models, the changes in ASV may display a different picture. The number of extra-tropical cyclones decreases by 3–5% under climate change in idealized OpenIFS experiments²² and CMIP6 simulations²³. Storm tracks shift poleward^{23–26} in the Pacific Ocean region in CMIP5 climate projections, decreasing kinetic energy (KE) in the subtropics especially in boreal winter²⁶. Consistently, a seasonal decrease in the synoptic anticyclone occurrence in midlatitudes has been shown in CMIP5 models²⁷. The net annual change in KE, especially at sea surface level, is however not clear due to the different methodologies employed and the strong seasonal variability. The future evolution of tropical cyclones occurrence is still unclear as future trends are strongly model-dependent^{28–30}. Furthermore, differences in the genesis potential index depend on the methodology employed³¹.

Here we assess the specific role of the long term integrated impact of a future change of ASV on ocean properties and biogeochemical cycles based on coupled atmosphere–ocean model experiments.

¹GEOMAR Helmholtz Centre for Ocean Research Kiel, Kiel, Germany. ²Center for Climate Physics, Institute for Basic Science (IBS), Busan, Republic of Korea. ³Department of Climate System, Pusan National University, Busan, Republic of Korea. ✉email: oduteil@geomar.de

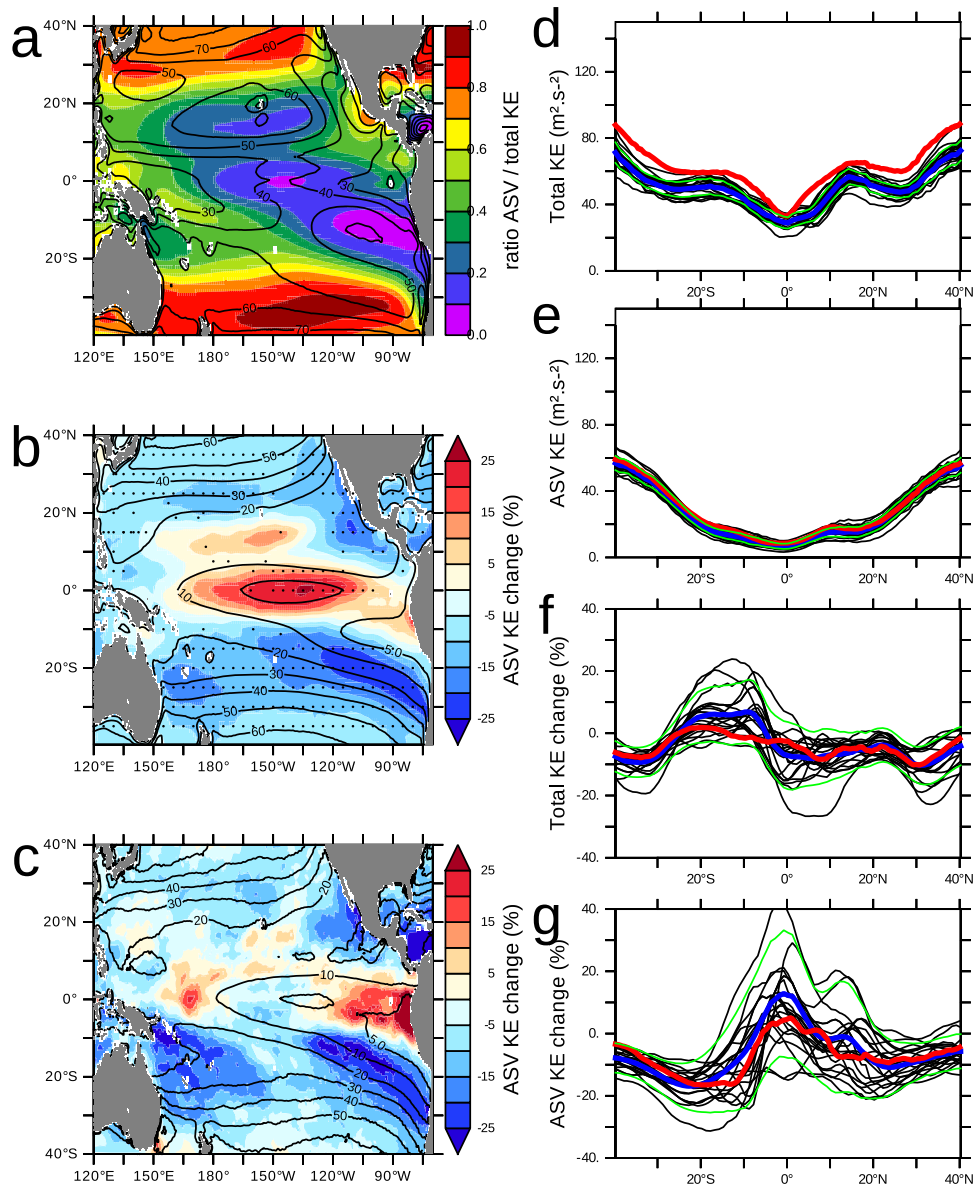


Fig. 1 Current and future atmospheric synoptic variability in climate models. **a** Fraction of the kinetic energy (KE) due to the atmospheric synoptic variability (ASV) in the ensemble of CMIP6 models (average 1980–2100) (See Table 1). Contour is the total KE ($\text{m}^2 \text{s}^{-2}$). **b** Change in ASV (percent) in the ensemble of CMIP6 models (model mean for the average period 2080–2100 compared to 1980–2000). Contour is the average 1980–2000 average ASV ($\text{m}^2 \text{s}^{-2}$). Dots are regions where more than 80% of the models agree on the sign of change. **c** ASV KE change (average years 120–140 compared to years 0–20) in the KCM. Contour is the ASV average of years 0–20 ($\text{m}^2 \text{s}^{-2}$). **d** Total KE zonal mean ($\text{m}^2 \text{s}^{-2}$) (average 1980–2000). **e** Similar to **(d)** but ASV KE is considered. **f** Changes average (2080–2100) in total KE compared to the present day (%). **g** Changes in ASV KE compared to the present day (%). In **(d–f)**, the black lines are individual CMIP6 models, the blue line is the average of CMIP6 models, the green lines are the average of CMIP6 models \pm one standard deviation, and the red line is the KCM. In all figures, the average annual ASV is considered.

RESULTS

Current and future KE of ASV in climate projections

The mean KE (Fig. 1a) of the considered CMIP6 models for the period 1980–2100 reaches maximal values of $40\text{--}50 \text{ m}^2 \text{ s}^{-2}$ in subtropical gyres between 20°S/N and 40°S/N while minimum values ($30 \text{ m}^2 \text{ s}^{-2}$) are located in the equatorial regions. The easterly trade winds are located at around 20° and are characterized by local maximums of $70 \text{ m}^2 \text{ s}^{-2}$. The ASV component (Fig. 1a) represents a large part of the total KE in mid-latitudes (about $50\text{--}60 \text{ m}^2 \text{ s}^{-2}$ equivalent to 70–80% of total KE north of 30°N/S). In the tropics, the relative importance of the ASV in the total KE is the smallest ($10\text{--}20 \text{ m}^2 \text{ s}^{-2}$ or $<30\%$). A similar pattern has been found previously³² in a study which quantified in

a model the relative importance of the wind sub-seasonal (60 days) variance. A minimum ($\text{KE} < 5 \text{ m}^2 \text{ s}^{-2}$) occurs in the tropical eastern Pacific Ocean. These results are in agreement with a previous study⁸, which quantified the variance of the wind speed in different frequencies and in particular in the “storm band” (18 h–1 month) in the ERA5 dataset. The mean spatial pattern of the Kiel Climate Model (KCM; see “Methods”) that is used in this study is consistent with the considered ensemble of CMIP6 models. The winds are however generally stronger in the KCM by about 10–20% (Fig. 1d).

Climate change impacts the total wind KE (Fig. 1f). In the southern tropical Pacific Ocean, KE increases as a result of the strengthening of the southern trade winds which extend toward

the western part of the basin³³. Total KE decreases in the Northern Hemisphere, especially at the rim of the high-latitude westerlies, which shift poleward due to the expansion of the Hadley cell³⁴.

The changes in the ASV component (Fig. 1b, c, g) are characterized by an annual mean decrease of 15% in the subtropical gyres, consistent with previous work²³. Similarly, a decrease in synoptic anticyclone occurrence in mid-latitudes has been shown in CMIP5²⁷. By the end of this century, climate models' projections display a poleward shift of mid-latitude storm tracks^{23–26}. Despite a strong seasonal variability²⁶, it translates here into an annual mean increase of KE by up to $10 \text{ m}^2 \text{ s}^{-2}$ (about 10%) in high latitude and a decrease in the subtropical regions (equatorward of about 40°) by a similar magnitude (similar to results obtained using CMIP3 models³⁵). Conversely, ASV increases by up to 20% in the equatorial band. The changes are consistent among the models studied here and in KCM-GW (Fig. 1g).

Sensitivity of ocean circulation to changes in ASV

Model experiments have been performed to assess the impact of the future change in ASV on upper ocean properties (see “Methods” and Table 2). In GW (“final state,” corresponding to the average of the past 10 years of the simulation, see “Methods”), mixed layer (ML) shallows by about 15% between 10°S and 10°N compared to CTL (from 37 m (CTL) to 33 m (GW)) and by about 20% between 20°S and 40°S (from 52 m (CTL) to 45 m (GW)). ML shallowing of the same magnitude order has been shown in CMIP5² and CMIP6 models⁴. Changes in ASV modulate the ML depth. Maintaining the ASV to current values (GW-ASVCTL minus GW) leads to a deepening of the ML in subtropical regions by 5–15% compared to GW (Fig. 2a). Conversely, it shallows at the equator by about 10%. Concomitantly, the SST decreases in GW-ASVCTL by $0.1\text{--}0.3^\circ\text{C}$, both in the subtropics and the tropical regions (Fig. 2b). Decreasing (GW-ASVM20, GW-ASVM10) or increasing ASV (GW-ASVP20, GW-ASVP10) leads to a linear ($R^2 = 0.99$) ML shallowing, associated with a SST decrease or increase (Fig. 2e, f). Several mechanisms are at play to explain these changes, acting at large (extra equatorial) and local (equatorial) scales.

Gyre-scale circulation determines the stratification background and the properties of the equatorial water upwelled. It is related to the meridional subtropical cells (STC)^{36–41}, which connect the subtropics to the tropics and extend to about 300 m depth. Equatorward to the STCs, tropical cells (TC) are strong and shallow (50 m) recirculation cells located between 5° and 10° . These cells are related to upper ocean mixing⁴² and the recirculation of water originating from the equatorial upwelling. They are therefore indirectly forced by large-scale wind patterns.

We define the strength of the STC and the TC here following Eqs. (1) and (2) (see “Methods”). Consistently to previous studies^{39,43,44}, the strength of both STC and TC decreases under global warming. Their strength is, respectively, 76 Sv (TC) and 60 Sv (STC) in CTL, while it declines to, respectively, 62 Sv (–19%) (TC) and 40 Sv (–33%) (STC) in GW. Compared to GW, the experiment GW-ASVCTL is characterized by an increase of 8 Sv (+10%) (TC) and 4 Sv (+10%) (STC). The strengthening of the upwelling in GW-ASVCTL is consistent with a decrease in SST by 0.1°C in the eastern tropical Pacific Ocean.

The relationship between ASV intensity, TC (STC) strength, and SST is clearly identified in Fig. 3a, b: in the experiment GW-ASVM20, where ASV is decreased by 20%, TC and STC strength decrease, respectively, to 58 Sv (–4%) and 39 Sv (–4%) associated with a 0.15°C increase compared to GW-ASVCTL. The experiment GW-ASVP20 displays the opposite picture. This result is consistent with a previous study⁴¹, which showed that the strength of the TC and STC controls the tropical SST over a long (decadal) time scale.

In complement to the change in circulation strength, an increase in ASV results in a deepening of the ML in the subtropics

and a cooling of the surface ocean due to an increase in the mixing depth. The increased subduction rate of water masses tends to deepen isopycnals. This mechanism contributes to providing cooler water to the equatorial regions, by subduction and transport of cooler water by the STCs. However, previous studies have shown that equatorial temperature anomalies are mostly due to changes in velocities and streamfunction rather than changes in subducted water properties⁴⁵.

Local mechanisms impact the water column stability and the upper ocean mixing with the deeper layer. This is particularly relevant in the Pacific equatorial upwelling as competition occurs between upwelling strength (reinforced by a strong ASV, as seen above) and vertical mixing of warm surface water with cold deeper water (also reinforced by a strong ASV, as the mixing depth directly depends on the wind KE). In complement, local equatorial winds generate Kelvin waves, modulating equatorial thermocline depth^{46,47} and SST. Furthermore, the wind velocity term plays a major role in determining the turbulent heat fluxes and SST in most of the tropical oceans with the exception of the equatorial upwelling^{48,49} where the heat fluxes are driven by the ocean–atmosphere gradient (and consequently the upwelling strength).

The relative importance of these competitive mechanisms is illustrated in Fig. 3. The experiment GW-ASVCTL displays an SST anomaly close to GW-ASVP20, which is consistent as ASV is stronger outside of the equator in GW-ASVCTL compared to GW. The strength of TC and STC are similar in GW-ASVCTL and GW-ASVP20. However, the ML shallows in GW-ASVCTL compared to GW while it deepens in GW-ASVP20, suggesting a local equatorial effect. We performed a complementary experiment GW-ASVCTL-FLX similar to GW-ASVCTL, but where the wind forcing the heat fluxes have been set to CTL values. Comparing GW-ASVCTL and GW-ASVCTL-FLX (Fig. 2c, d) shows clearly that while the changes in heat fluxes have a dominant effect in subtropical regions, the change in circulation is dominant to explain changes in the equatorial regions.

Sensitivity of net primary production to changes in ASV

Net primary productivity (NPP) displays the highest values (greater than $300 \text{ gC m}^{-2} \text{ yr}^{-1}$) in tropical regions and in the eastern boundary upwelling system. Values are intermediate ($50\text{--}100 \text{ gC m}^{-2} \text{ yr}^{-1}$) in the subtropical system and minimum in the subtropical gyres (less than $50 \text{ gC m}^{-2} \text{ yr}^{-1}$). Previous analyses of CMIP5 and CMIP6 experiments have shown a global mean NPP decline from -2 to -18% in 2100 compared to 2000 in CMIP5 (RCP 8.5 scenario)² and CMIP6 models (SSR850 scenario)⁴. Comparing the final state of the experiments GW and CTL shows that the total Pacific Ocean NPP decreases from about 12 to 10.5 GtC yr^{-1} (–15%) in GW.

Productivity is strongly related to stratification in the tropical Pacific Ocean⁵⁰ as an increase of the upper layer stratification reduces the exchanges between the upper, nutrient-poor, and lower, nutrient-rich, ocean. Increasing or decreasing the ASV may modulate the upper ocean stratification and consequently nutrient availability in the mixed layer. The stratification changes due to global warming are related both to changes in the mixed layer, caused by changes in heat fluxes or vertical mixing depth, and to changes in the deeper ocean circulation linked with changes in the wind-driven TC/STCs. The role of ocean circulation in controlling NPP is illustrated in Fig. 4, showing the correlation between the NPP low frequency variability in the tropical Pacific Ocean and the TC (Fig. 4a, b), STC (Fig. 4c, d) and ML depth (Fig. 4e, f). At low frequency, the NPP is most strongly correlated to the TC, directly linked to the upper equatorial upwelling system, and the STC: a stronger TC and STC result in an increase of NPP, by transporting more nutrients to the euphotic zone. In complement, NPP correlates to a lower extent with the mixed layer depth, as a

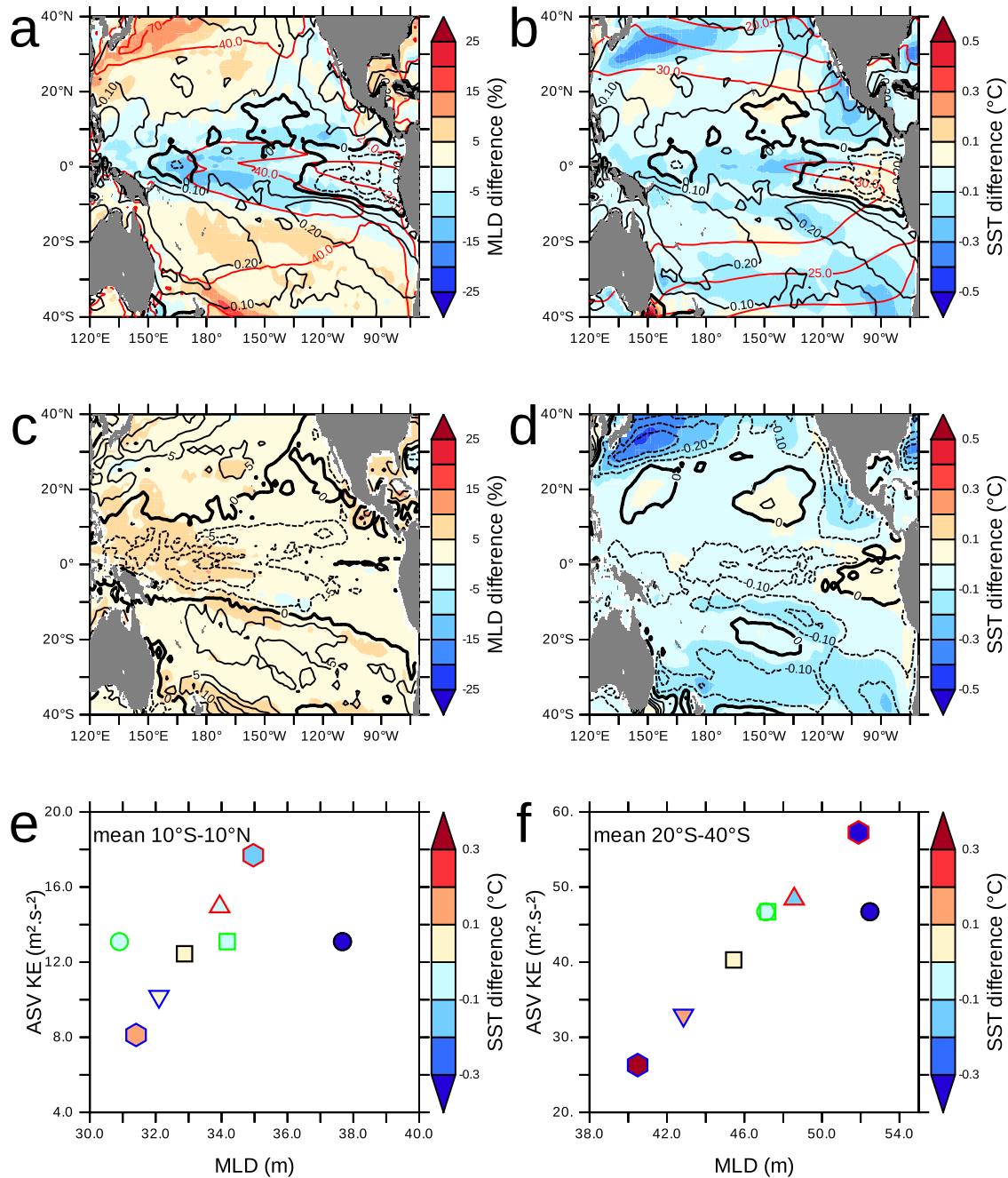


Fig. 2 ASV change, sea surface temperature, and mixed layer depth. **a** Mixed layer depth (MLD) difference (percent) between GW-ASVCTL and GW (GW-ASVCTL minus GW). The ASV kinetic energy (KE) difference is represented in black contour. The average GW MLD (m) is represented in red contour. **b** Sea surface temperature (SST) difference ($^{\circ}\text{C}$) between GW-ASVCTL and GW. The ASV kinetic energy difference is represented in black contour. The average SST ($^{\circ}\text{C}$) is represented in red contour. **c** Mixed layer depth (MLD) difference (percent) between GW-ASVCTL-FLX and GW. The MLD difference (percent) between GW-ASVCTL and GW is represented in contour. **d** Average SST difference ($^{\circ}\text{C}$) between GW-ASVCTL-FLX and GW. The SST difference ($^{\circ}\text{C}$) between GW-ASVCTL and GW is represented in contour. **e, f** The region 10°N - 10°S (**e**) and 20°S - 40°S (**f**) are considered. The mean MLD (m; abscissa) vs. KE ASV (m^2s^{-2} ; ordinate) vs. SST anomaly compared to GW-ASVCTL (color) for each experiment are represented. The black circle represents the experiment CTL, the black square GW, the green circle GW-ASVCTL, the green square GW-ASVCTL-FLX (the ASV value corresponding to GW-ASVCTL is plotted here), the blue triangle GW-ASVM10, the blue hexagon GW-ASVM20, the red triangle GW-ASVP10, and the red hexagon GW-ASVP20 (see Table 2 for experiments).

deeper ML is associated with more mixing with the nutrient-rich deep ocean in the tropical regions.

Maintaining the ASV to current values (GW-ASVCTL) leads to an increase in NPP compared to GW in the regions of strong productivity (Fig. 5a). The most prominent increase occurs in the tropical Pacific Ocean (up to $50\text{ gC m}^{-2}\text{ yr}^{-1}$). Total NPP in the Pacific Ocean is equal to about 10.5 GtC yr^{-1} in GW-ASVCTL, which

corresponds to a decrease of solely about 15% compared to CTL and only half of the decrease modeled in GW (Fig. 5b): changes in ASV contribute to half of the change in NPP due to climate change. The relationship between ASV intensity and NPP change is clearly shown by the linear correlation ($R^2 = 0.97$) between ASV intensity (experiments GW-ASVP10, GW-ASVP20, GW-ASVM10, GW-ASVM20) and NPP (Fig. 5b). NPP increase in GW-ASVCTL in a

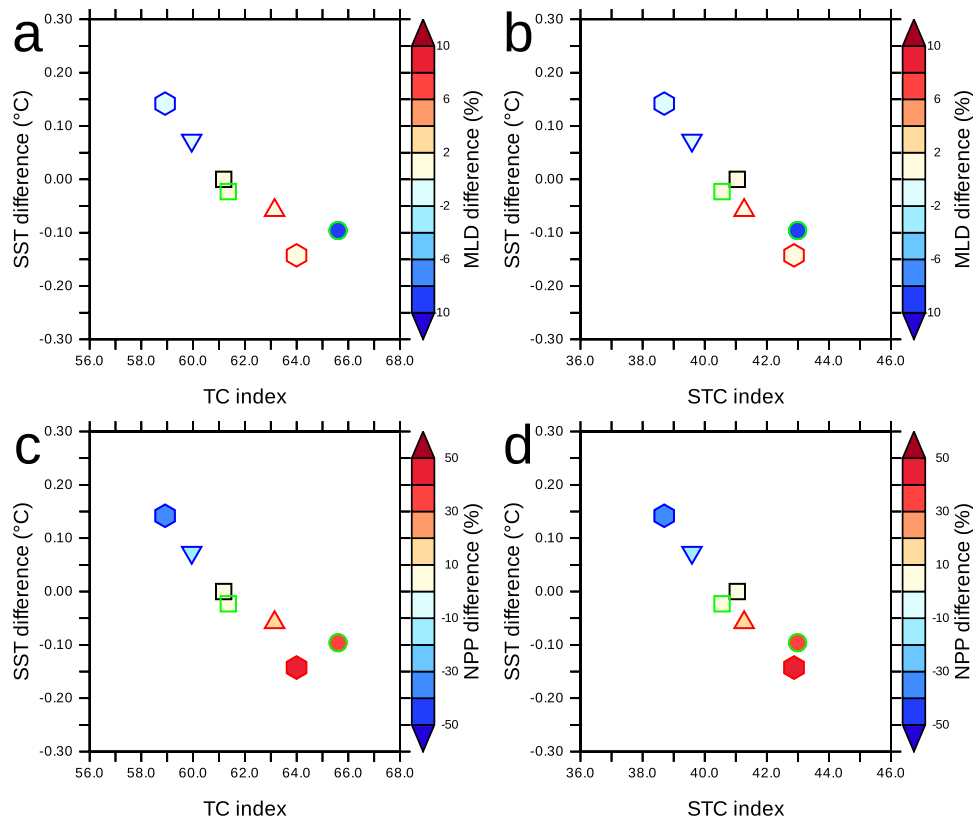


Fig. 3 Subtropical/tropical cells index and upper ocean properties. **a, b** Mean sea surface temperature difference (10°N – 10°S) ($^{\circ}\text{C}$) (compared to GW) vs. Tropical Cells Index (**a**) (see “Methods”) and Subtropical Cells Index (**b**). The mixed layer depth (MLD) difference (m) (10°N – 10°S) is shown in color for each experiment. **c, d** Similar to (**a, b**) but net primary production (NPP) difference (percent) (compared to GW) is shown in color for each experiment. The black square is GW, green circle GW-ASVCTL, green square GW-ASVCTL-FLX, blue triangle GW-ASVM10, blue hexagon GW-ASVM20, red triangle GW-ASVP10, red hexagon GW-ASVP20 (see Table 2 for a list of the experiments).

similar way as in GW-ASVP10, despite a shallowing of the ML in GW-ASVCTL, suggesting the impact of ASV-related changes in the strength of the TC/STC are dominant (Fig. 3c, d) compared to changes in the mixed layer depth.

DISCUSSION

We quantified in this study the impact of the ASV, more specifically of the wind forcing, on ocean circulation and NPP. While this impact is implicitly considered in forced (the atmospheric field resolution of reanalysis is of the order of 1 h) or coupled models, its integrated global-scale impact has not been explicitly quantified in a climate change context.

A simple methodology has been used to define the atmospheric synoptic variability based on a band-pass filter approach. This filter permits isolating frequencies higher than 30 days, as the band 12–30 days is considered the lowest frequency of variability at the synoptic timescale²². Such a 30-day threshold has been used in previous studies to isolate synoptic variability^{19,26,51,52}.

In CMIP6 models the mean KE contained in the ASV band (0–30 days) represents more than half of the total mean average KE poleward of 20° . The annual mean KE in the ASV band decreases due to climate change in the subtropical regions, corresponding to a reduction of storminess. Conversely, the annual mean ASV KE increases in the equatorial region. Using the Kiel Climate Model, we performed model experiments to assess the long-term impact of the change in ASV on ocean upper properties in a climate change context. Compared to a control global warming experiment, maintaining ASV at current values leads to a shallowing of the ML in the tropics and a deepening in the subtropics, associated with a strengthening of the wind-driven

tropical (TCs) and subtropical–tropical cells (STCs) and an increase in net primary productivity. Increasing or decreasing ASV has a linear effect on the strength of these recirculation cells. The TCs/STCs connect the subduction regions, the equatorial undercurrent system and the equatorial upwelling. They play a large role in SST^{36–41} and biogeochemical variability⁵³ of the equatorial ocean, especially at decadal timescale³⁶. Climate models however still do not agree on their mean state and on the magnitude of future changes⁴¹. Current and future changes in ASV need to be explicitly quantified in climate projections, as they may partly explain some of the inter-model heterogeneity.

This study opens up further questions. It has been previously shown that changes in ASV impacts the productive Eastern Boundary Upwelling Systems (EBUS)^{54,55} by modifying local upwelling favorable winds patterns⁵⁶. In complement, a change in large-scale circulation and thus equatorial connections^{57,58} may have an impact on these productive areas. ASV changes may also modify the mean state of other biogeochemical quantities such as oxygen concentrations. Observations have shown an oxygen decrease in the interior ocean⁵⁹, fostering the expansion of Oxygen Minimum Zones^{60,61} impacting marine life and biogeochemical cycles. Climate models do not agree on the oxygen decline and even the sign of change^{2,4,62}. Oxygen levels depend on solubility, transport, and productivity^{53,62,63}. All these mechanisms are potentially impacted by ASV changes. Finally, by modulating the ocean mean state ASV changes may have an impact on the amplitude of the El Niño/Southern Oscillation (ENSO) due to ocean/atmosphere feedbacks^{64,65}. We therefore advocate for a more thorough assessment of ASV in climate models.

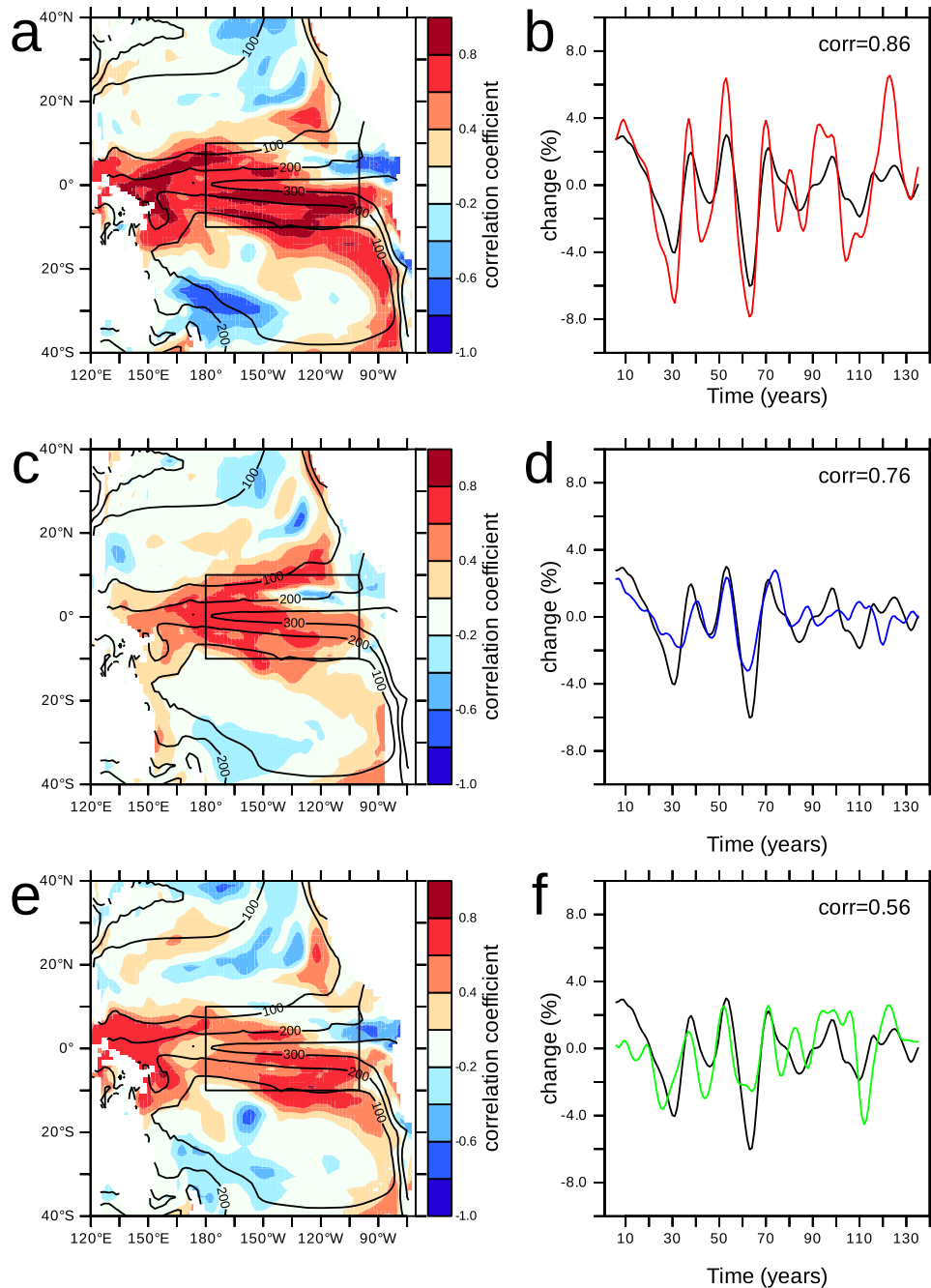


Fig. 4 Net primary production low frequency variability and ocean circulation. **a** Correlation coefficient between net primary production (NPP) and Tropical Cells (TC) Index (11 years running mean) (see “Methods”). **b** Time series of NPP (black) and TC index (11 years running mean) in the region (180°E–100°E, 10°N–10°S). **c, d** Similar to (a, b) but considering subtropical cells (STC). **e, f** Similar to (a, b) but considering mixed layer depth (MLD). The experiment analyzed is CTL (see Table 2). The region 180°W–100°W, 10°N–10°S is considered in (b, d, f).

METHODS

Climate models

We analyzed a subset of 20 CMIP6 models (ssp585 scenario) (Table 1) as well as a high-resolution (T255 spectral, approximately 50 km) experiment⁶⁶ of the Kiel Climate Model (KCM)³⁹ characterized by a 1% CO₂ increase per year (KCM-GW).

We isolate the low-frequency (LF) and the high-frequency synoptic variability (ASV) part of the zonal and meridional 10 m wind fields by applying a 30 days low-pass filter after having detrended the data. The temporal resolution of the CMIP6 outputs used here is 1 day, while the temporal resolution of the KCM outputs is 12 h.

Forced ocean–biogeochemistry experiments

We assess specifically the role of a change in ASV on ocean properties by using an ocean–biogeochemistry model (NEMO-PISCES)⁶⁷. For that purpose, atmospheric forcings sets are constructed from KCM experiments in a first step, and used to force the NEMO-PISCES experiments in a second step.

Construction of atmosphere forcing sets from the KCM

The atmosphere forcings sets are constructed based on two high-resolution experiments (T255 spectral, approximately 50 km)⁶⁶ performed using KCM. The experiment KCM-GW is characterized

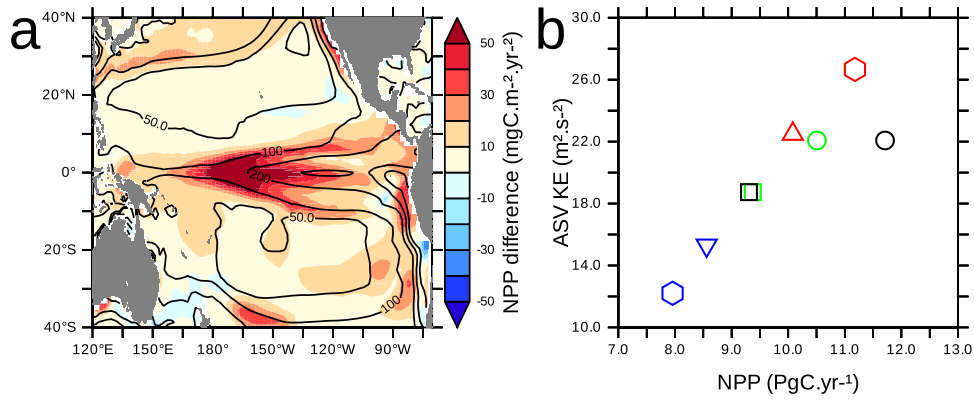


Fig. 5 ASV changes and net primary production. **a** Difference in depth-integrated net primary production (NPP) ($\text{mgC m}^{-2} \text{yr}^{-1}$) between GW-ASVCTL and GW. The mean NPP in GW is displayed in contour. **b** ASV kinetic energy ($\text{m}^2 \text{s}^{-2}$) vs. total NPP (PgC yr^{-1}) in the Pacific Ocean. Black square is GW, green circle GW-ASVCTL, green square GW-ASVCTL-FLX (the ASV value corresponding to GW is plotted here), blue triangle GW-ASVM10, blue hexagon GW-ASVM20, red triangle GW-ASVP10, and red hexagon GW-ASVP20 (see Table 2 for experiments).

Table 1. Resolution of the ocean and atmosphere components of CMIP6 and KCM models used in this study.

Model	Ocean	Atmosphere
ACCESS-CM2	360 × 300 (1° with refinement in the tropics)	192 × 144 (N96)
AWI-CM-1-1-MR	Unstructured	384 × 192 (T127)
BCC-CSM2-MR	360 × 232 (1° with refinement to 0.3° in the tropics)	320 × 160 (T106)
CanESM5	361 × 290 (1° with refinement to 0.3° in the tropics)	128 × 64 (T63)
CMCC-CM2-SR5	362 × 292 (1° with refinement to 0.3° in the tropics)	288 × 192
EC-Earth3	362 × 292 (1° with refinement to 0.3° in the tropics)	512 × 256 (linearly reduced T255)
EC-Earth3-Veg	362 × 292 (1° with refinement to 0.3° in the tropics)	512 × 256 (linearly reduced T255)
GFDL-CM4	1440 × 1080 (0.25°)	360 × 180 (1°)
GFDL-ESM4	720 × 576 (0.5°)	360 × 180 (1°)
IITM-ESM	360 × 200 (1°)	192 × 94 (linearly reduced T62)
INM-CM4-8	360 × 318 (1° with refinement in the tropics)	180 × 120 (2° × 1.5°)
INM-CM5-0	720 × 720 (0.5° × 0.25°)	180 × 120 (2° × 1.5°)
IPSL-CM6A-LR	362 × 332 (1°)	144 × 143 (N96)
KACE-1-0-G	360 × 200 (1°)	192 × 144 (N96)
KIOST-ESM	360 × 200 (1°)	192 × 96 (Cubed sphere C48)
MIROC6	360 × 256 (1°)	256 × 128 (T255)
MPI-ESM1-2-HR	802 × 404 (0.4°)	384 × 192 (T127)
MPI-ESM1-2-LR	256 × 220 (1.5°)	192 × 96 (T63)
MRI-ESM2-0	360 × 364 (1° with refinement 10°S–10°N up to 0.3°)	320 × 160 (linearly reduced T159)
NESM3	384 × 362 (1° × 0.5°)	192 × 96 (T63)
KCM	182 × 149 (2° with refinement to 0.5° in the tropics)	768 × 384 (T255)

Table 2. Summary of the NEMO-PISCES experiments performed in this study.

Experiment name	Forcing name	ASV-part from	LF-part from
CTL	F-CTL	KCM-CTL	KCM-CTL
GW	F-GW	KCM-GW	KCM-GW
GW-ASVCTL	F-GW-ASVCTL	KCM-CTL	KCM-GW
GW-ASVCTL-FLX	F-GW (dynamics) F-GW-ASVCTL (heat fluxes)	KCM-GW (dynamics) KCM-CTL (heat fluxes)	KCM-GW
GW-ASVP10	F-GW-ASVP10	KCM-GW + 10%	KCM-GW
GW-ASVP20	F-GW-ASVP20	KCM-GW + 20%	KCM-GW
GW-ASVM10	F-GW-ASVM10	KCM-GW – 10%	KCM-GW
GW-ASVM20	F-GW-ASVM20	KCM-GW – 20%	KCM-GW

by a 1% CO₂ increase per year and has been compared to CMIP6 models in this study. After 140 years of integration, CO₂ levels reach 4 times the initial concentration in KCM-GW. The experiment KCM-CTL is characterized by a constant pCO₂ level of 348 ppm. Both experiments are initialized from a spun-up simulation with a CO₂ level of 348 ppm and integrated for 140 years. The temporal resolution of the outputs used to construct the forcings is 12 h.

The forcing sets constituted by meridional and zonal winds at 10 m height (u10, v10), air temperature at 10 m height (t10), humidity at 10 m height (q10), sea level pressure (SLP), precipitation (PRE), short- and long-wave fluxes (QSR and QLW) have been constructed:

—F-GW: the forcings originate from the experiment KCM-GW

—F-CTL: the forcings originate from the experiment KCM-CTL

—F-GW-ASVCTL: the LF part of u10, v10 originates from KCM-GW, while the ASV part originates from KCM-CTL. t10, q10, SLP, PRE, QSR, and QLW originate from F-GW

—F-GW-ASVM10, F-GW-ASVM20, F-GW-ASVP10, F-GW-ASVP20: the LF and the ASV part of u10, v10 originate from KCM-GW. The ASV part has been, respectively, decreased by −10%, −20% and increased by +10%, +20%. t10, q10, SLP, PRE, QSR, and QLW originate from F-GW.

Ocean–biogeochemistry NEMO-PISCES experiments

To determine the importance of changes in ocean circulation and biogeochemistry, we performed 140-years-long sensitivity tests (Table 2) using the ocean general circulation model NEMO coupled to a biogeochemical model of intermediate complexity, PISCES⁶⁷. The atmospheric forcing sets are described above. The ORCA2 configuration, characterized by a nominal 2° horizontal resolution (refined to 0.5° meridionally in the tropics) with 31 vertical levels has been used. The ocean resolution is comparable to that of the CMIP6 analyzed models and permits us to estimate the role of the ASV in climate projections. This NEMO-PISCES framework has been used in previous studies^{19,67}.

The surface fluxes have been computed using the same methodology employed by a previous study¹⁹. A damping term has been added to the freshwater flux for stability reasons. The “final state” of the experiments (average of years 130–140) is compared in this study.

Subtropical (STC) and Tropical Cells (TC) Index

The TC and STC Index have been defined similarly to previous studies^{37,39}.

$$TC = \psi_{\max}(5^{\circ}S - 5^{\circ}N, \text{upper } 250 \text{ m}) - \psi_{\min}(5^{\circ}S - 5^{\circ}N, \text{upper } 250 \text{ m}) \quad (1)$$

$$STC = \psi_{\max}(10^{\circ}N - 30^{\circ}N, \text{upper } 250 \text{ m}) - \psi_{\min}(10^{\circ}S - 30^{\circ}S, \text{upper } 250 \text{ m}) \quad (2)$$

where ψ_{\max} and ψ_{\min} are the maximal and minimal values of the Meridional Overturning Streamfunction in the given latitude and depth ranges.

DATA AVAILABILITY

The model experiment data are available at <https://figshare.com/s/2cab684cfc34dceca6f>. The outputs of the CMIP6 models are available at <https://esgf-data.dkrz.de/projects/cmip6-dkrz/>.

CODE AVAILABILITY

The code of the ocean model is NEMOv4.0. It includes PISCESv2. The code is available at <https://forge.nemo-ocean.eu/nemo>.

Received: 31 January 2023; Accepted: 18 August 2023;

Published online: 08 September 2023

REFERENCES

- IPCC. *IPCC Climate Change 2021. The Physical Science Basis* (Cambridge University Press, 2023).
- Bopp, L. et al. Multiple stressors of ocean ecosystems in the 21st century: projections with CMIP5 models. *Biogeosciences* **10**, 6225–6245 (2013).
- Fu, W., Randerson, J. T. & Moore, J. K. Climate change impacts on net primary production (NPP) and export production (EP) regulated by increasing stratification and phytoplankton community structure in the CMIP5 models. *Biogeosciences* **13**, 5151–5170 (2016).
- Kwiatkowski, L. et al. Twenty-first century ocean warming, acidification, deoxygenation, and upper-ocean nutrient and primary production decline from CMIP6 model projections. *Biogeosciences* **17**, 3439–3470 (2020).
- Tagliabue, A. et al. Persistent uncertainties in ocean net primary production climate change projections at regional scales raise challenges for assessing impacts on ecosystem services. *Front. Clim.* **3**, 738224 (2021).
- Gulev, S. K., Jung, T. & Ruprecht, E. Climatology and interannual variability in the intensity of synoptic-scale processes in the North Atlantic from the NCEP-NCAR reanalysis data. *J. Clim.* **15**, 809–828 (2002).
- Ruane, A. C. & Roads, J. O. 6-Hour to 1-year variance of five global precipitation sets. *Earth Interactions* **11**, 1–29 (2007).
- West, C. G. & Smith, R. B. Global patterns of offshore wind variability. *Wind Energy* **24**, 1466–1481 (2021).
- Ulbrich, U., Leckebusch, G. C. & Pinto, J. G. Extra-tropical cyclones in the present and future climate: a review. *Theor. Appl. Climatol.* **96**, 117–131 (2009).
- Savazzi, A. C. M., Nuijens, L., Sandu, I., George, G. & Bechtold, P. The representation of the trade winds in ECMWF forecasts and reanalyses during EUREC 4 A. *Atmos. Chem. Phys.* **22**, 13049–13066 (2022).
- Wang, C. & Magnusdottir, G. The ITCZ in the Central and Eastern Pacific on synoptic time scales. *Mon. Weather Rev.* **134**, 1405–1421 (2006).
- Brown, J. R. et al. South Pacific Convergence Zone dynamics, variability and impacts in a changing climate. *Nat. Rev. Earth Environ.* **1**, 530–543 (2020).
- Haffke, C. & Magnusdottir, G. The South Pacific Convergence Zone in three decades of satellite images. *J. Geophys. Res. Atmos.* **118**, 10,839–10,849 (2013).
- Yan, Y., Song, X., Wang, G. & Chen, C. Importance of high-frequency (≤ 30 -day) wind variability to the annual climatology of the surface latent heat flux inferred from the global tropical moored buoy array. *JGR Oceans* **127**, e2021JC018094 (2022).
- Menkes, C. E. et al. Global impact of tropical cyclones on primary production. *Glob. Biogeochem. Cycles* **30**, 767–786 (2016).
- Fujii, M. & Yamanaka, Y. Effects of storms on primary productivity and air-sea CO₂ exchange in the subarctic western North Pacific: a modeling study. *Biogeosciences* **5**, 1189–1197 (2008).
- Nicholson, S.-A. et al. Storms drive outgassing of CO₂ in the subpolar Southern Ocean. *Nat. Commun.* **13**, 158 (2022).
- Wu, Y., Zhai, X. & Wang, Z. Impact of synoptic atmospheric forcing on the mean ocean circulation. *Journal of Climate* **29**, 5709–5724 (2016).
- Duteil, O. Wind synoptic activity increases oxygen levels in the tropical Pacific ocean. *Geophys. Res. Lett.* **46**, 2715–2725 (2019).
- Dobrynin, M., Murawsky, J. & Yang, S. Evolution of the global wind wave climate in CMIP5 experiments. *Geophys. Res. Lett.* **39**, L18606 (2012).
- Deng, K., Azorin-Molina, C., Minola, L., Zhang, G. & Chen, D. Global near-surface wind speed changes over the last decades revealed by reanalyses and CMIP6 model simulations. *J. Clim.* **34**, 2219–2234 (2021).
- Sinclair, V. A., Rantanen, M., Haapanala, P., Räisänen, J. & Järvinen, H. The characteristics and structure of extra-tropical cyclones in a warmer climate. *Weather Clim. Dynam.* **1**, 1–25 (2020).
- Priestley, M. D. K. & Catto, J. L. Future changes in the extratropical storm tracks and cyclone intensity, wind speed, and structure. *Weather Clim. Dynam.* **3**, 337–360 (2022).
- Chang, E. K. M., Guo, Y. & Xia, X. CMIP5 multimodel ensemble projection of storm track change under global warming. *J. Geophys. Res.* **117**, D23118 (2012).
- Tamarin, T. & Kaspi, Y. The poleward shift of storm tracks under global warming: a Lagrangian perspective. *Geophys. Res. Lett.* **44**, 10,666–10,674 (2017).
- Chemke, R. The future poleward shift of Southern Hemisphere summer mid-latitude storm tracks stems from ocean coupling. *Nat. Commun.* **13**, 1730 (2022).
- Pepler, A. Projections of synoptic anticyclones for the twenty-first century. *Clim. Dyn.* **61**, 3271–3287 (2023).

28. Knutson, T. R. et al. Global projections of intense tropical cyclone activity for the late twenty-first century from dynamical downscaling of CMIP5/RCP4.5 scenarios. *J. Clim.* **28**, 7203–7224 (2015).
29. Emanuel, K. Evidence that hurricanes are getting stronger. *Proc. Natl Acad. Sci. USA* **117**, 13194–13195 (2020).
30. Vecchi, G. A. et al. Tropical cyclone sensitivities to CO₂ doubling: roles of atmospheric resolution, synoptic variability and background climate changes. *Clim. Dyn.* **53**, 5999–6033 (2019).
31. Murakami, H. & Wang, B. Patterns and frequency of projected future tropical cyclone genesis are governed by dynamic effects. *Commun. Earth Environ.* **3**, 77 (2022).
32. Whitt, D. B., Nicholson, S. A. & Carranza, M. M. Global impacts of subseasonal (<60 day) wind variability on ocean surface stress, buoyancy flux, and mixed layer depth. *J. Geophys. Res. Oceans* **124**, 8798–8831 (2019).
33. Li, Y. et al. Long-term trend of the tropical Pacific trade winds under global warming and its causes. *J. Geophys. Res. Oceans* **124**, 2626–2640 (2019).
34. Grise, K. M. & Davis, S. M. Hadley cell expansion in CMIP6 models. *Atmos. Chem. Phys.* **20**, 5249–5268 (2020).
35. O’Gorman, P. A. Understanding the varied response of the extratropical storm tracks to climate change. *Proc. Natl Acad. Sci. USA* **107**, 19176–19180 (2010).
36. McPhaden, M. J. & Zhang, D. Slowdown of the meridional overturning circulation in the upper Pacific Ocean. *Nature* **415**, 603–608 (2002).
37. Lohmann, K. & Latif, M. Tropical Pacific decadal variability and the subtropical–tropical cells. *J. Clim.* **18**, 5163–5178 (2005).
38. Lübbecke, J. F., Böning, C. W. & Biastoch, A. Variability in the subtropical-tropical cells and its effect on near-surface temperature of the equatorial Pacific: a model study. *Ocean Sci.* **4**, 73–88 (2008).
39. Park, W. et al. Tropical Pacific climate and its response to global warming in the Kiel climate model. *J. Clim.* **22**, 71–92 (2009).
40. Farneti, R., Dwivedi, S., Kucharski, F., Molteni, F. & Griffies, S. M. On Pacific subtropical cell variability over the second half of the twentieth century. *J. Clim.* **27**, 7102–7112 (2014).
41. Graffino, G., Farneti, R. & Kucharski, F. Low-frequency variability of the Pacific subtropical cells as reproduced by coupled models and ocean reanalyses. *Clim. Dyn.* **56**, 3231–3254 (2021).
42. Lu, P., McCreary, J. P. & Klingler, B. A. Meridional circulation cells and the source waters of the Pacific equatorial undercurrent. *J. Phys. Oceanogr.* **28**, 62–84 (1998).
43. Wang, D. & Cane, M. A. Pacific shallow meridional overturning circulation in a warming climate. *J. Clim.* **24**, 6424–6439 (2011).
44. Heede, U. K., Fedorov, A. V. & Burls, N. J. Time scales and mechanisms for the tropical Pacific response to global warming: a tug of war between the ocean thermostat and weaker walker. *J. Clim.* **33**, 6101–6118 (2020).
45. Nonaka, M. Decadal variations in the subtropical cells and equatorial Pacific SST. *Geophys. Res. Lett.* **29**, 2001GL013717 (2002).
46. Dewitte, B., Purca, S., Illig, S., Renault, L. & Giese, B. S. Low-frequency modulation of intraseasonal equatorial Kelvin wave activity in the Pacific from SODA: 1958–2001. *J. Clim.* **21**, 6060–6069 (2008).
47. Rydbeck, A. V., Jensen, T. G. & Flatau, M. Characterization of intraseasonal Kelvin waves in the equatorial Pacific Ocean. *J. Geophys. Res. Oceans* **124**, 2028–2053 (2019).
48. Small, R. J., Bryan, F. O., Bishop, S. P. & Tomas, R. A. Air–sea turbulent heat fluxes in climate models and observational analyses: what drives their variability? *J. Clim.* **32**, 2397–2421 (2019).
49. Sun, X. & Wu, R. Contribution of wind speed and sea-air humidity difference to the latent heat flux–SST relationship. *Ocean Land Atmos Res.* **2022**, 9815103 (2022).
50. Behrenfeld, M. J. et al. Climate-driven trends in contemporary ocean productivity. *Nature* **444**, 752–755 (2006).
51. Löptien, U. & Ruprecht, E. Effect of synoptic systems on the variability of the North Atlantic Oscillation. *Mon. Weather Rev.* **133**, 2894–2904 (2005).
52. Pérez-Santos, I. et al. Synoptic-scale variability of surface winds and ocean response to atmospheric forcing in the eastern austral Pacific Ocean. *Ocean Sci.* **15**, 1247–1266 (2019).
53. Duteil, O., Böning, C. W. & Oschlies, A. Variability in subtropical-tropical cells drives oxygen levels in the tropical Pacific Ocean. *Geophys. Res. Lett.* **41**, 8926–8934 (2014).
54. Chavez, F. P. & Messié, M. A comparison of eastern boundary upwelling ecosystems. *Prog. Oceanogr.* **83**, 80–96 (2009).
55. García-Reyes, M. et al. Under pressure: climate change, upwelling, and eastern boundary upwelling ecosystems. *Front. Mar. Sci.* **2**, 109 (2015).
56. Aguirre, C., Rojas, M., Garreaud, R. D. & Rahn, D. A. Role of synoptic activity on projected changes in upwelling-favourable winds at the ocean’s eastern boundaries. *npj Clim. Atmos. Sci.* **2**, 44 (2019).
57. Illig, S. et al. Forcing mechanisms of intraseasonal SST variability off central Peru in 2000–2008. *J. Geophys. Res.* **119**, 3548–3573 (2014).
58. Montes, I., Colas, F., Capet, X. & Schneider, W. On the pathways of the equatorial subsurface currents in the eastern equatorial Pacific and their contributions to the Peru-Chile Undercurrent. *J. Geophys. Res.* **115**, C09003 (2010).
59. Schmidtko, S., Stramma, L. & Visbeck, M. Decline in global oceanic oxygen content during the past five decades. *Nature* **542**, 335–339 (2017).
60. Stramma, L., Johnson, G. C., Sprintall, J. & Mohrholz, V. Expanding oxygen-minimum zones in the tropical oceans. *Science* **320**, 655–658 (2008).
61. Breitburg, D. et al. Declining oxygen in the global ocean and coastal waters. *Science* **359**, eaam7240 (2018).
62. Oschlies, A. et al. Patterns of deoxygenation: sensitivity to natural and anthropogenic drivers. *Philos. Trans. R. Soc. A* **375**, 20160325 (2017).
63. Cabré, A., Marinov, I., Bernardello, R. & Bianchi, D. Oxygen minimum zones in the tropical Pacific across CMIP5 models: mean state differences and climate change trends. *Biogeosciences* **12**, 5429–5454 (2015).
64. Bayr, T. & Latif, M. ENSO atmospheric feedbacks under global warming and their relation to mean-state changes. *Clim. Dyn.* **60**, 2613–2631 (2023).
65. Cai, W. et al. Changing El Niño–Southern Oscillation in a warming climate. *Nat. Rev. Earth Environ.* **2**, 628–644 (2021).
66. Park, W. & Latif, M. Resolution dependence of CO₂-induced Tropical Atlantic sector climate changes. *npj Clim. Atmos. Sci.* **3**, 36 (2020).
67. Aumont, O., Ethé, C., Tagliabue, A., Bopp, L. & Gehlen, M. PISCES-v2: an ocean biogeochemical model for carbon and ecosystem studies. *Geosci. Model Dev.* **8**, 2465–2513 (2015).

ACKNOWLEDGEMENTS

O.D. acknowledges support from the DFG (Deutsch Forschungsgemeinschaft) (project “SyVarBio” – 434479332). W.P. acknowledges support from IBS (IBS-R028-D1). The model experiments have been performed at HLRN (North German Supercomputing Alliance) and at the Christian Albrecht University (CAU Kiel, Germany) computing Center.

AUTHOR CONTRIBUTIONS

O.D.: funding acquisition, methodology, analysis, writing (original draft, review and editing). W.P.: methodology, writing (review and editing).

FUNDING

Open Access funding enabled and organized by Projekt DEAL.

COMPETING INTERESTS

The authors declare no competing interests.

ADDITIONAL INFORMATION

Correspondence and requests for materials should be addressed to Olaf Duteil.

Reprints and permission information is available at <http://www.nature.com/reprints>

Publisher’s note Springer Nature remains neutral with regard to jurisdictional claims in published maps and institutional affiliations.



Open Access This article is licensed under a Creative Commons Attribution 4.0 International License, which permits use, sharing, adaptation, distribution and reproduction in any medium or format, as long as you give appropriate credit to the original author(s) and the source, provide a link to the Creative Commons license, and indicate if changes were made. The images or other third party material in this article are included in the article’s Creative Commons license, unless indicated otherwise in a credit line to the material. If material is not included in the article’s Creative Commons license and your intended use is not permitted by statutory regulation or exceeds the permitted use, you will need to obtain permission directly from the copyright holder. To view a copy of this license, visit <http://creativecommons.org/licenses/by/4.0/>.

© The Author(s) 2023